Taming Driftwave Turbulence: Numerical Simulations and Experiment

V. Naulin[1], Christiane Schröder[2], Thomas Klinger[2], Dietmar Block[3], Alexander Piel[3], Gerard Bonhomme[4] and S.B. Korsholm[1]

[1] *Association EURATOM – Risø National Laboratory Optics and Fluid Dynamics Department, OFD-128 Risø, 4000 Roskilde, Denmark*

[2] *Institut für Physik, Ernst-Moritz-Arndt Universität Greifswald, Germany*

[3] *Institut für Experimentelle und Angewandte Physik, Christian-Albrechts Universität Kiel, Germany*

[4] *Laboratoire de physique des millieux ionisés, Université Henri Poincaré Nancy, France*

Abstract Driftwave turbulence in a linear cylindrical plasma is influenced by applying a spatiotemporal signal to a number of exciter plates near the edge of the plasma. Numerical simulations of that process are presented and a fully nonlocal nonlinear model for the plasma presented.

Experiments are carried out in the linear, low-β plasma devices KIWI[2] and MIRABELLE[1]. They consist of two plasma source chambers and a magnetized midsection (data for MIRABELLE: length 1.4 m, diameter 0.30 m, magnetic field $B = 40 - 100\,\mathrm{mT}$). Argon plasma is produced in the source chambers by thermionic hot-cathode discharge in steady-state operation (neutral gas pressure $p = 3 \cdot 10^{-4}\,\mathrm{mbar}$, electron temperature $T_e = 1.2 - 3.5\,\mathrm{eV}$, electron density $n_e = 2 \cdot 10^{16}\,\mathrm{m}^{-3}$). The source chambers are separated from the mid-section by stainless-steel mesh grids. One chamber is operated as plasma source and the grid there is biased. In this way electrons are injected into the mid-section and, to a certain degree, an $E \times B$-rotation of the plasma column is established [2]. Increasing U_g leads to a transition scenario from a stable plasma state to drift wave turbulence. The spatio-temporal drift wave dynamics is observed using an array of 32 equally spaced cylindrical Langmuir probes [3] (Fig. 1). Fully developed drift wave turbulence is achieved by choosing $U_g = 5\,\mathrm{V}$ (Figs. 4(a)-(d) top). The time trace of the floating potential fluctuations (a) is clearly irregular and the corresponding frequency power spectrum $S(f)$ is broad-band (b), even though a few pronounced peaks are visible in the low-frequency regime ($f < f_{ci} = 15\,\mathrm{kHz}$, the ion cyclotron frequency). The spatio-temporal data (c) is dominated by irregular features and no clear-cut mode structure is observed [2]. Developed turbulence is further corroborated by the frequency-modenumber spectrum $S(f, m)$, shown in subfigure (d). Spectral components are scattered over a broad area in the (f, m)-plane and show no unique dispersion relation. For synchronization of the turbulence, a driver frequency f_d is chosen close to pronounced spectral features in the low-frequency regime. An azimuthal mode number m_d is determined by selecting a phase shift $\theta = m_d\,\pi/4$. The exciter signal drives a specific drift mode with phase velocity $v_\phi = f_d \cdot 2\pi r_x/m_d$. r_x is the radial position of the exciter electrodes. Choosing $m_d = 2$, frequency $f_d = 8.0\,\mathrm{kHz}$, and amplitude $A = 1.0\,\mathrm{V}$ the drift wave turbulence is successfully synchronized as shown in Figs. 4(e)-(h). The floating potential fluctuations (e) are now fairly regular and have a relatively large amplitude, of the order of the largest events in

the turbulent state [cf. Fig. 4(a)]. The frequency power spectrum (f) is sharply peaked at 8.06 kHz and its higher harmonics only, meaning that the preselected mode is enhanced to the expense of broad-band low-frequency spectral components. The spectral index $f^{-\alpha}$ of the broad-band high-frequency underground ($f \geq f_{ci} = 15\,\mathrm{kHz}$, small-scale) drops from $\alpha = 4.2$ to $\alpha = 3.5$. Synchronization increases the integrated fluctuation power by a factor of 5.7, mainly due to the driven mode as the power of the broad-band part is significantly decreased. Regular dynamics dominate the spatio-temporal data (g) as well. A pronounced wave structure with mode number $m = 2$ is found, which is also present in the sharply peaked frequency-modenumber spectrum $S(f, m)$. This emphasizes the mode-selective character of the spatio-temporal control. To test the control effect we reverse the rotation direction of the exciter field as we expect a much weaker influence for counter-rotating excitation. Fig. 4(i)-(m) shows the result. Indeed, the counter-rotating exciter field has almost no influence on the drift wave turbulence (see also Figure 1). In conclusion, the interaction between the counter-rotating exciter field and the drift wave turbulence is weak, as expected. 3D modeling using the drift approximation and quasi-neutrality leads with $\ln n = N$ to:

$$\begin{aligned} \frac{d}{dt}\nabla^2\phi &= \mu\nabla^4\phi - \nabla N \cdot \left(\frac{d}{dt}\nabla\phi + \nu\nabla\phi - \mu\nabla\nabla^2\phi\right) \\ &\quad -\tau\nabla_\parallel^2(\phi - N) - \tau\nabla_\parallel N\nabla_\parallel(\phi - N) - U_0\nabla_\parallel N - \nu\nabla^2\phi \end{aligned} \tag{1}$$

$$d_t N = -\tau\nabla_\parallel^2(\phi - N) - \tau\nabla_\parallel N\nabla_\parallel(\phi - N) - U_0\nabla_\parallel N \tag{2}$$

A finite parallel electron drift U_0 is responsible for the instability: Linearizing around a Gaussian density profile, introducing $\nu_e = \tau k_\parallel^2$, $w_1 = U_0 k_\parallel$, and $b = k^2$ the growth-rate is given via

$$\omega_i = \frac{\omega^\star}{\tau(1+k^2)}\left(\frac{k^2\omega^\star}{(1+k^2)^2} + w_1\right) - \frac{k^2}{1+k^2}(\nu_i + \mu k^2) \tag{3}$$

The drift dissipative instability (terms proportional to $\frac{\omega^\star}{\nu_e}$) is dwarfed against the axial current instability for $w_1 > \omega^\star$. The typical evolution of the global system is started from a Gaussian density profile being fixed at the lower axial boundary. The system undergoes a fast relaxation during which a global potential sets up. For parameters corresponding to the experiment we get the following results from the numerical simulations, performed on a 64x64x12 cylindrical grid with a timestep $\Delta t = 0.002$ corresponding to approximately

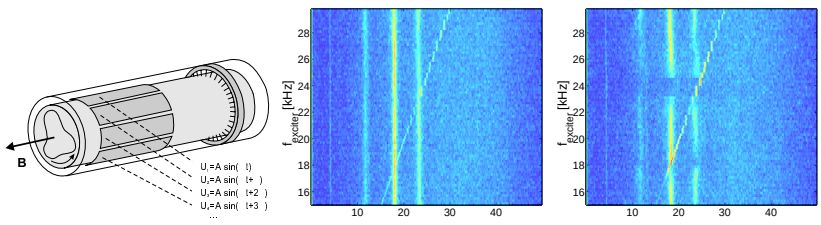

Figure 1: The exciter (left): eight plates of length 32 cm with radius $r_x = 10\,\mathrm{cm}$ and azimuthal Langmuir probe array. Middel and right: Frequency spectrum of fluctuations with an m=3 mode at varying driver frequency, counter- (middle) and co-rotating (right).

1/100 μs: To ease numerical simulations we consider a reduced 2D model keeping the parallel current explicitly:

$$\frac{\partial}{\partial t}\nabla_\perp^2\phi + \vec{V}_E\cdot\nabla\nabla_\perp^2\phi = \nabla_\parallel J_\parallel + \mu_w\nabla_\perp^4\phi\ ;\quad \frac{\partial}{\partial t}n + \vec{V}_E\cdot\nabla(N_0+n) = \nabla_\parallel J_\parallel + \mu_n\nabla_\perp^2 n \quad (4)$$

with $J_\parallel = -\sigma\nabla_\parallel(\phi - n)$. Here N_0 is the fixed background density. The exciter is modeled by assuming an oscillatory parallel current profile of the functional form $\nabla_\parallel J_{ext} = A\sin(\pi r/r_0)\sin(2\pi m_d\Theta - \omega_d t) = S$, where r_0 is the radius of the plasma and Θ is the poloidal coordinate. Making the transition to a 2d we use $\nabla_\parallel^2 \approx -k_\parallel^2$, and $\tilde{\sigma} = k_\parallel\sigma = k_\parallel^2\rho_s T_e/m_e c_s\nu_{ei}$. Additionally, in small layers around $r = 0$ and $r = r_0$ the viscosities are enhanced by a factor 200. These layers act as sources and sinks and sustain the background density gradient. Simulations are performed in poloidal co-ordinates on a disk, with typically up to 64×128 grid points in the radial and poloidal direction, respectively. The density profile is taken to be of the form $N_0 = 2.5\cos(r/r_0)$, with $r_0 = 10$ and the viscosities $\mu_{n,w}$ are of order 10^{-3} and $\tilde{\sigma} = 0.1$. The parameters are chosen to establish a saturated turbulent state similar to the experimentally observed one. Time series of the density and potential fluctuations are analyzed using the same diagnostic tools as for the experimental data. The simulation result is shown in Fig. 4. It is evident that the experimental findings discussed above are fully reproduced by the simulation. Starting with unperturbed drift wave turbulence (a)-(d), a synchronized $m = 2$ state is achieved at relatively small driver amplitude, $A = 0.75$, if a co-rotating current profile is applied (e)-(h). Exactly as in the experiment, a counter-rotating current profile of the same amplitude has almost no effect (i)-(m). The integrated spectral power and spectral indices behave similar to experiment. For synchronized turbulence, the integrated spectral power is increased by a factor of 5.5 and the spectral index α drops by a factor 2-3, stronger than in experiment. From numerical simulation we may conclude that that the experiment is at least qualitatively reproduced by the 2d model. The rotating current profile couples via $\nabla_\parallel J_{ext}$ the two equations mode-selectively and thus leads to amplification of the preselected mode m_d. In other words, in the drift wave frame the poloidal symmetry is broken by the structured current profile which leads to mode-selection. We note that only a rotating current profile yields synchronization; alternative concepts like rotating electric fields etc. gave no effect. Accessing transport in the numerics is rather tedious as the 2D setup picks up the transport at the location of the drive. Therefor

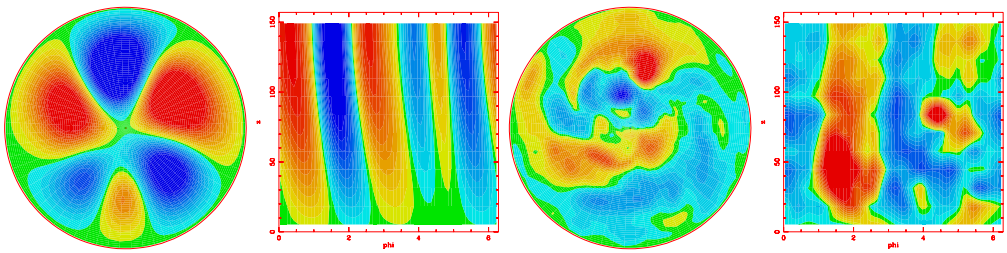

Figure 2: Density perturbations (radial-poloidal and polodal-axial) in the linear (left, 1μs after initialization maximum amplitude 1%) and in turbulent state (right, 60 μs after initialization maximum 25 %).

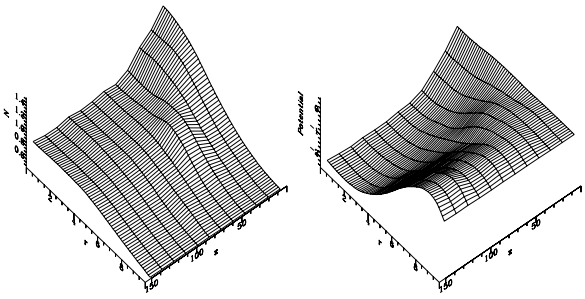

Figure 3: Density background (left) and background potential (right) in the nonlinear state.

transport estimates have to be made using the 3D model. Additional experimental and numerical difficulties arise due to the strong axial transport in the system. Thus accessing the transport is work in progress and preliminary results indicate that the transport can be modified, but as well transport reduction as transport amplification has been observed. The change of the transport is also dependent on the radial position of the measurement, what is in accordance with the intrinsic three dimensionality of the problem. Work is in progress on that issue.

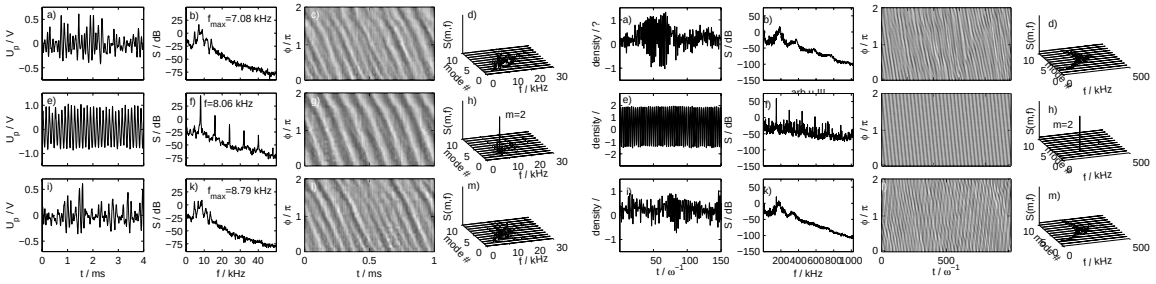

Figure 4: Drift wave dynamics: experiment (top) and simulation (bottom). The three rows each show: unperturbed case, co-rotating exciter field, and counter-rotating exciter field, respectively. The columns show: floating potential fluctuations, frequency power spectrum, spatiotemporal density fluctuations and frequency-modenumber power spectrum.

References

[1] T. Pierre, G. Leclert, and F. Braun, Rev. Sci. Instr. **58**, 6 (1987).

[2] T. Klinger, A. Latten, A. Piel, and G. Bonhomme, Plasma Phys. Controlled Fusion **39**, B145 (1997).

[3] A. Latten, T. Klinger, A. Piel, and T. Pierre, Rev. Sci. Instr. **66**, 3254 (1995).

[4] V. Naulin, K. H. Spatschek, S. Musher, and L. I. Piterbarg, Phys. Plasmas **2**, 2640 (1995).

[5] C. Schröder, Th. Klinger, D. Block, A. Piel, G. Bonhomme, V. Naulin, Phys. Rev. Lett. **86**, 5711-5714, 2001